

**Electronic supplementary information for**  
**“Carbon vacancy in  $Ti_2CT_2$  MXenes: defects or a new**  
**opportunity?”**

Tao Hu<sup>1,2</sup>, Jinxing Yang<sup>1,3</sup> and Xiaohui Wang<sup>1,\*</sup>

<sup>1</sup>Shenyang National Laboratory for Materials Science, Institute of Metal Research, Chinese Academy of Sciences, 72 Wenhua Road, Shenyang 110016, China

<sup>2</sup>University of Chinese Academy of Sciences, Beijing 100049, China

<sup>3</sup>School of Materials Science and Engineering, University of Science and Technology of China, Shenyang 110016, China

---

\*Corresponding author: wang@imr.ac.cn

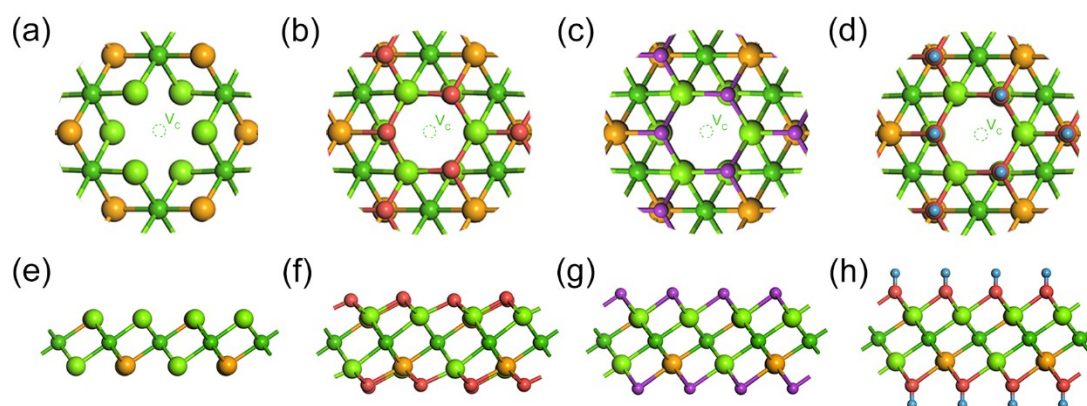


**Fig. S1** Optimized local crystal structure of carbon vacancy in  $Ti_2CT_2$  MXenes. (a)–(d) Top view and (e)–(h) side view of  $Ti_2C-V_C$ ,  $Ti_2CO_2-V_C$ ,  $Ti_2CF_2-V_C$  and  $Ti_2C(OH)_2-V_C$  monolayer. No structure reconstruction was found.

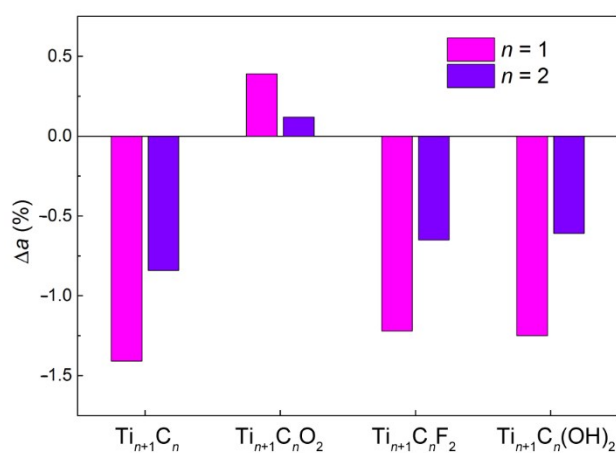


**Fig. S2** Changes of lattice constants  $a$  of  $Ti_{n+1}C_n-V_C$  and  $Ti_{n+1}C_nT_2-V_C$  ( $n = 1$  and  $2$ ,  $T = O, F, OH$ ). As the Ti–C frame work of  $Ti_3C_2T_2$  is more rigid,  $V_C$  imposes more influence on  $Ti_2CT_2-V_C$  than  $Ti_3C_2T_2-V_C$ .

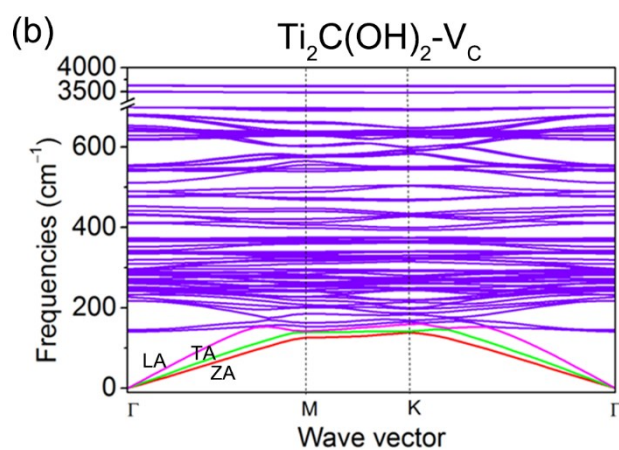
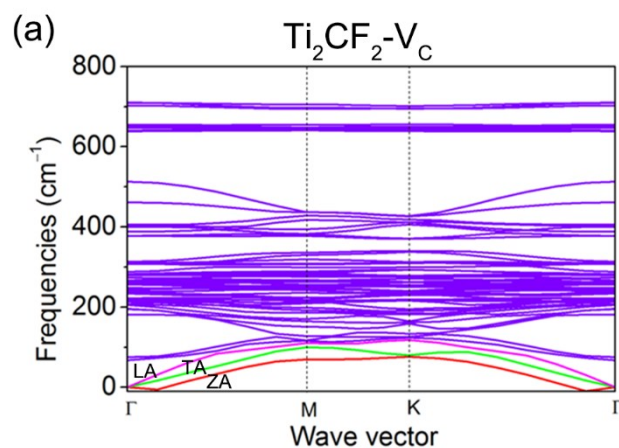


**Fig. S3** Phonon dispersions of  $\text{Ti}_2\text{CF}_2\text{-V}_\text{C}$  and  $\text{Ti}_2\text{C(OH)}_2\text{-V}_\text{C}$  monolayer.

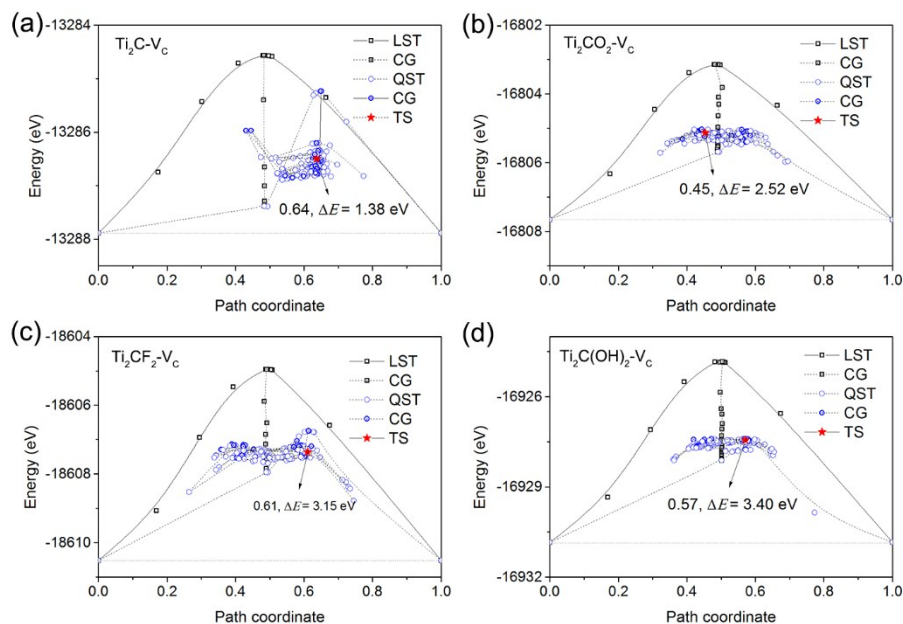


**Fig. S4** Transition state search process of (a)  $\text{Ti}_2\text{C-V}_\text{C}$ , (b)  $\text{Ti}_2\text{CO}_2\text{-V}_\text{C}$ , (c)  $\text{Ti}_2\text{CF}_2\text{-V}_\text{C}$  and (d)  $\text{Ti}_2\text{C(OH)}_2\text{-V}_\text{C}$  by LST/QST combined with CG methods.

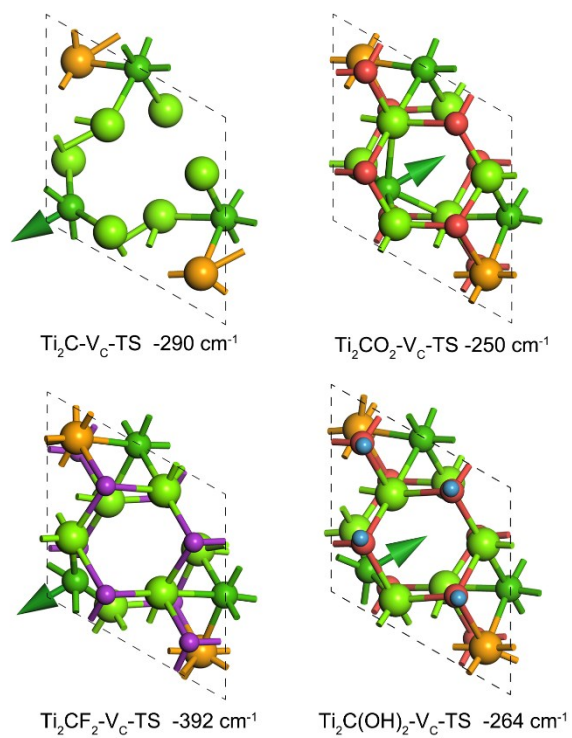


**Fig. S5** Imaginary frequency vibrational modes at gamma point in transition states of  $\text{V}_c$  migration in  $\text{Ti}_2\text{CT}_2\text{-V}_c$  ( $\text{Ti}_2\text{CT}_2\text{-V}_c\text{-TS}$ ). Note that the imaginary-frequency vibration modes are along the migration path. All other modes are positive, confirming that the transition states are accurately searched.

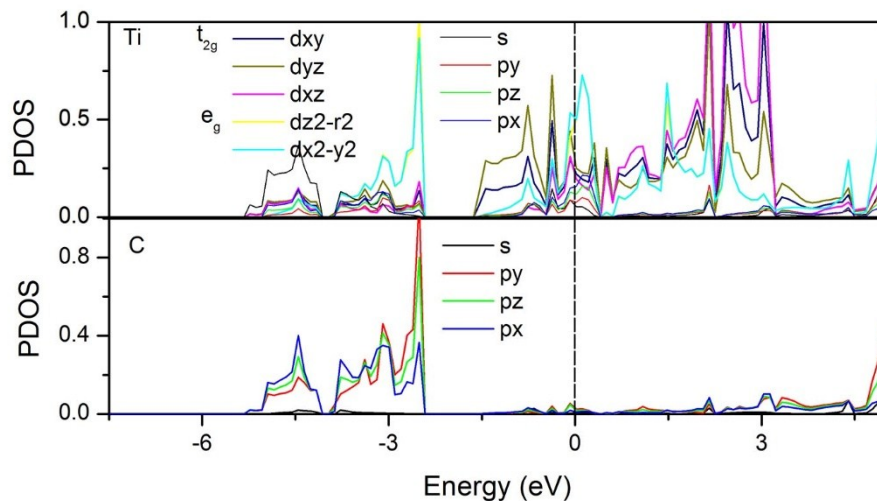


**Fig. S6a** Orbitally resolved projected DOS of Ti<sub>2</sub>C MXenes. The strong Ti-C bonds forms by *pd* hybridization, specifically speaking, C 2*p*-Ti 3*d* orbitals hybridization. Note that 5 orbitals of Ti split into two groups: *t*<sub>2*g*</sub> and *e*<sub>g</sub>.

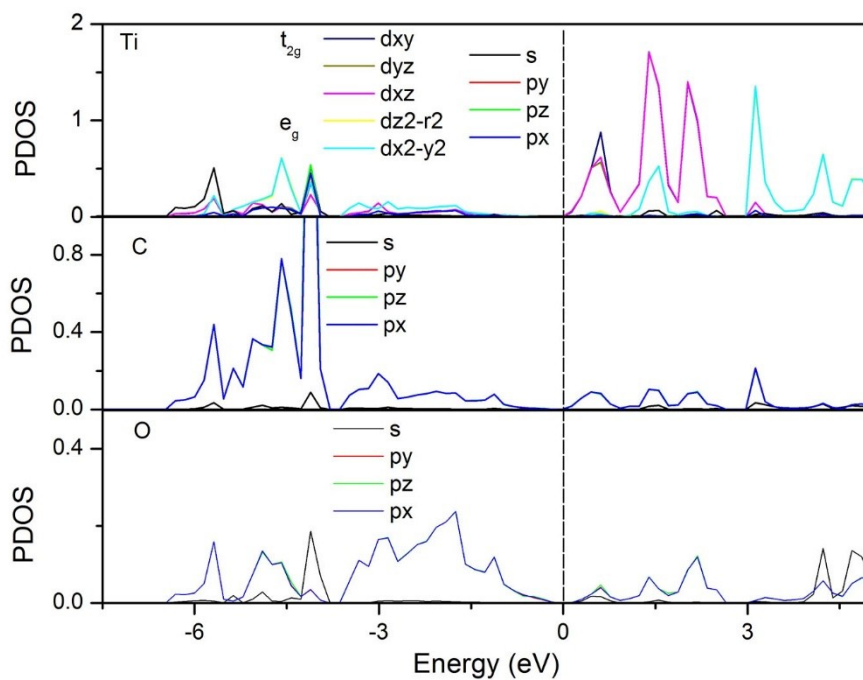


**Fig. S6b** Orbitally resolved projected DOS of Ti<sub>2</sub>CO<sub>2</sub> MXenes. The strong Ti-C bonds forms by *pd* hybridization, specifically speaking, C/O 2*p*-Ti 3*d* orbitals hybridization. Note that 5 orbitals of Ti split into two groups: *t*<sub>2*g*</sub> and *e*<sub>g</sub>.

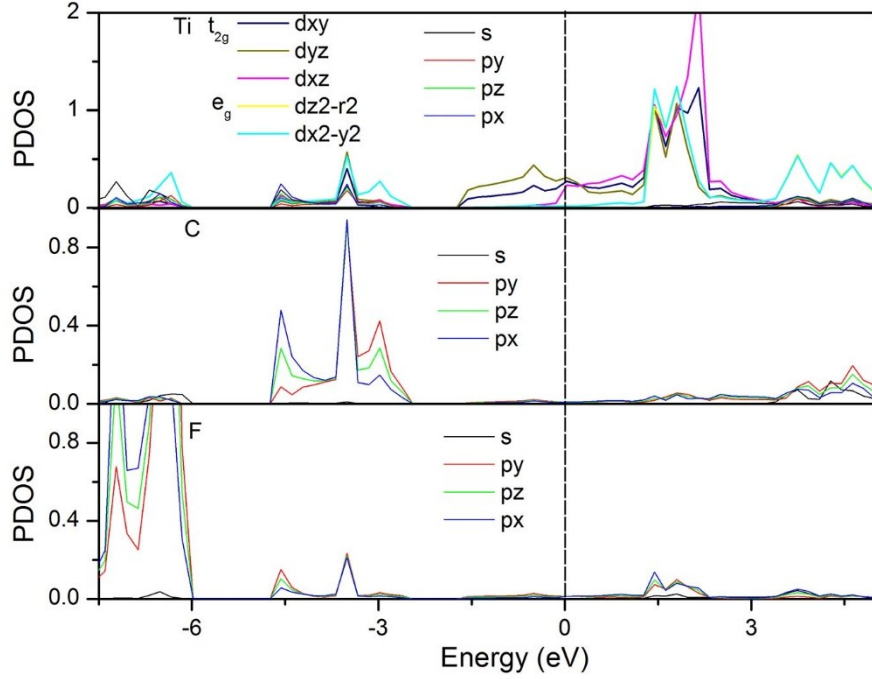


**Fig. S6c** Orbitally resolved projected DOS of  $\text{Ti}_2\text{CF}_2$  MXenes. The Ti-C bonds forms by  $pd$  hybridization, specifically speaking, C/F  $2p$ -Ti  $3d$  orbitals hybridization. Note that 5 orbitals of Ti split into two groups:  $t_{2g}$  and  $e_g$ .

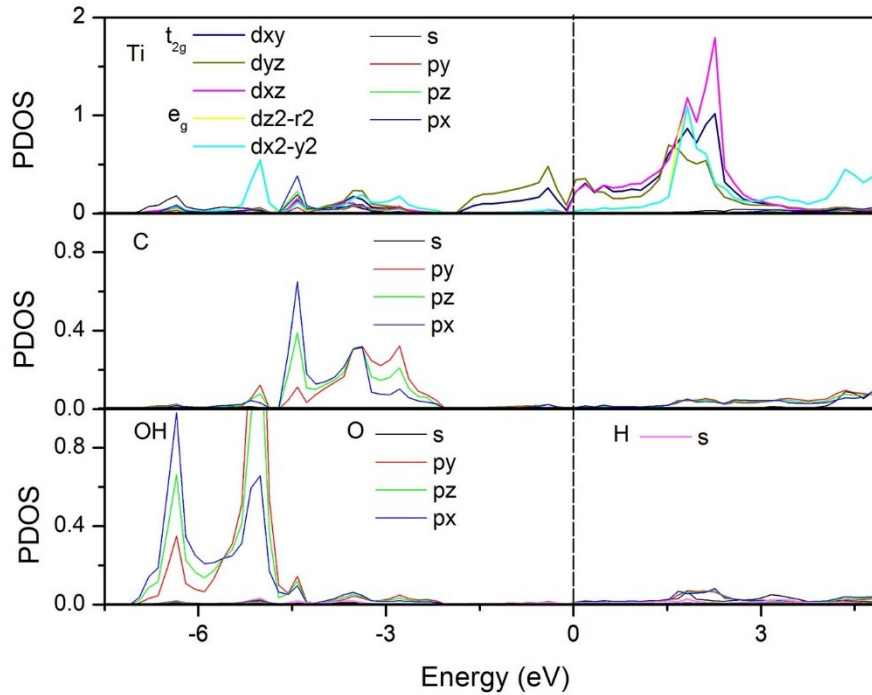


**Fig. S6d** Orbitally resolved projected DOS of  $\text{Ti}_2\text{C}(\text{OH})_2$  MXenes. The Ti-C bonds forms by  $pd$  hybridization, specifically speaking, C/OH  $2p$ -Ti  $3d$  orbitals hybridization. Note that 5 orbitals of Ti split into two groups:  $t_{2g}$  and  $e_g$ .

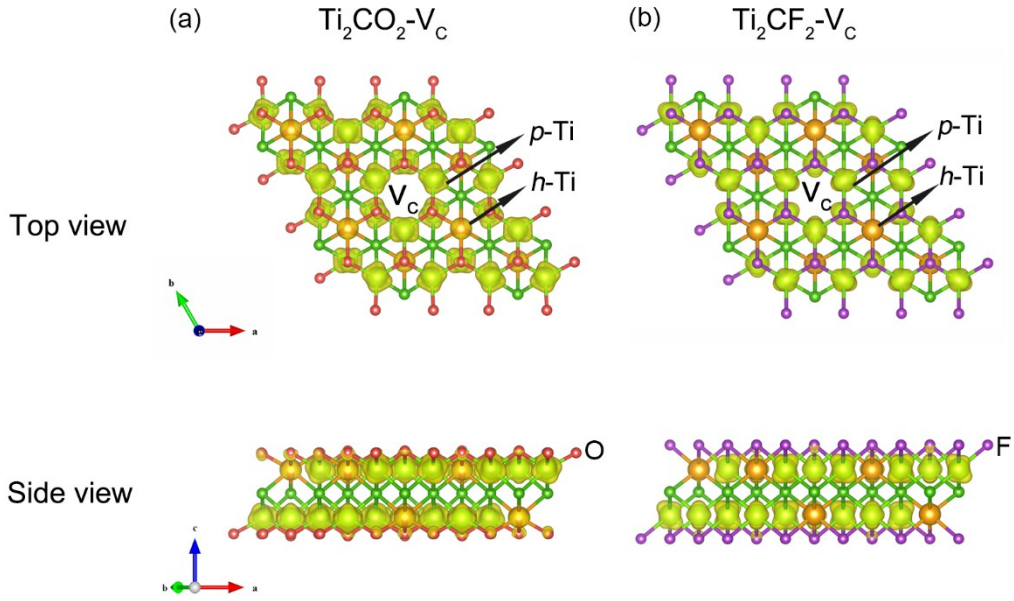


**Fig. S7** Band-decomposed chargedensity in the very vicinity of  $E_F$  ( $-0.1$  eV to  $0.1$  eV) of (a)  $\text{Ti}_2\text{CO}_2\text{-V}_c$  and (b)  $\text{Ti}_2\text{CF}_2\text{-V}_c$  using an isosurface of  $0.008$   $\text{e}/\text{\AA}^3$ . The localized states mainly come from the penta-coordinated  $p\text{-Ti}$  atoms enclosing the  $\text{V}_c$  and also some come from hexa-coordinated  $h\text{-Ti}$ . Besides, the shape of the band-decomposed chargedensity indicates that the localized states are  $t_{2g}$ -like orbitals.

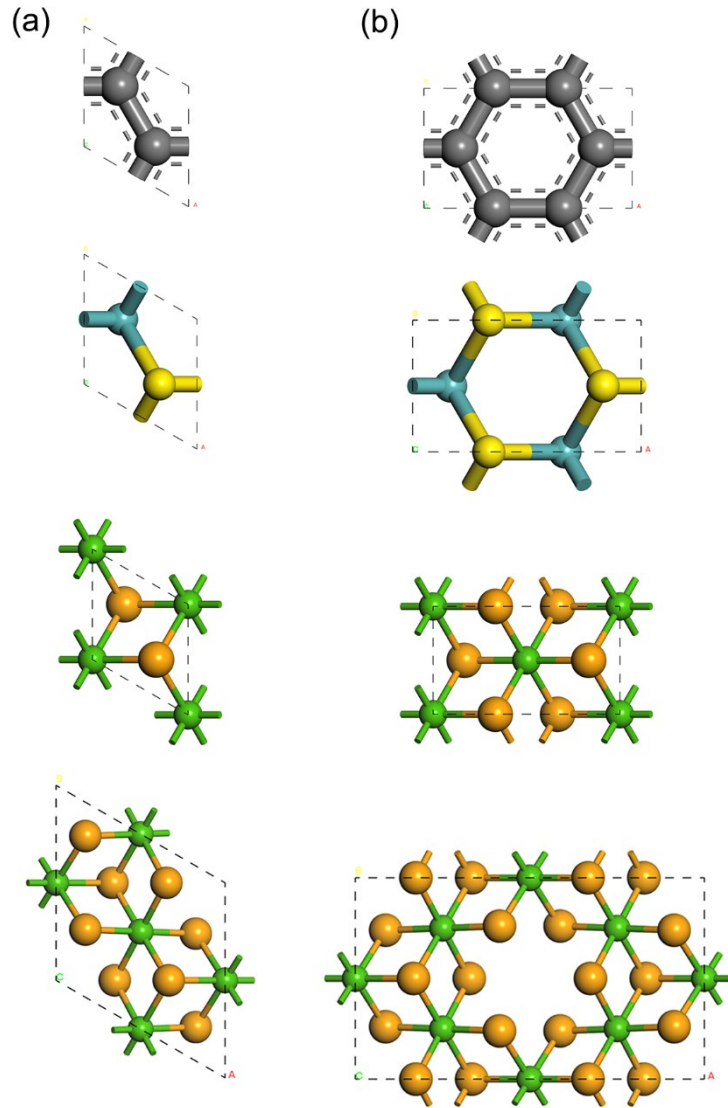


**Fig. S8** Schematic of (a) unit cell and (b) rectangular supercell configuration of the system used

for the calculation of the elastic constants. The transition matrix is  $\begin{bmatrix} 2 & 1 & 0 \\ 0 & 1 & 0 \\ 0 & 0 & 1 \end{bmatrix}$ .

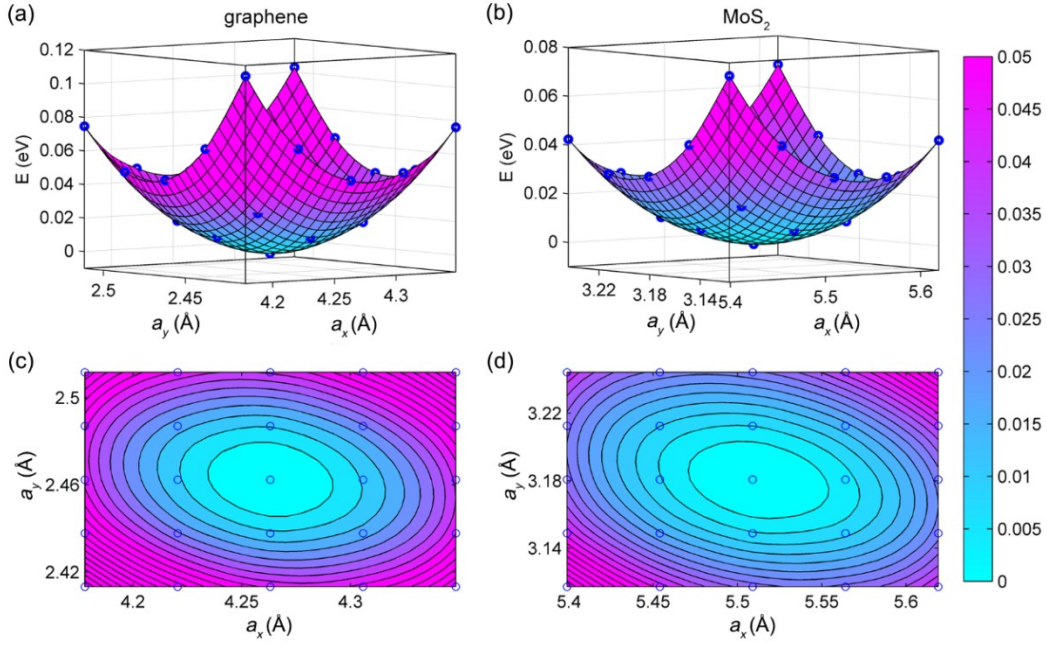


**Fig. S9** The three-dimensional plot of  $a_x$ ,  $a_y$  and corresponding strain energies of (a) graphene and (b)  $\text{MoS}_2$ . Contour of energy in the  $a_x$ - $a_y$  plane of (c) graphene and (d)  $\text{MoS}_2$ . For graphene,  $C = 337.8744$  N/m. This value is in a good agreement with earlier experimental and theoretical study. Our calculated value of the in-plane stiffness of graphene is in good agreement with the experimental value of  $340 \pm 50$  N/m and justifies the reliability of our method. For  $\text{MoS}_2$ ,  $C = 122.4$  N/m, agrees well with reported value of 123 N/m.

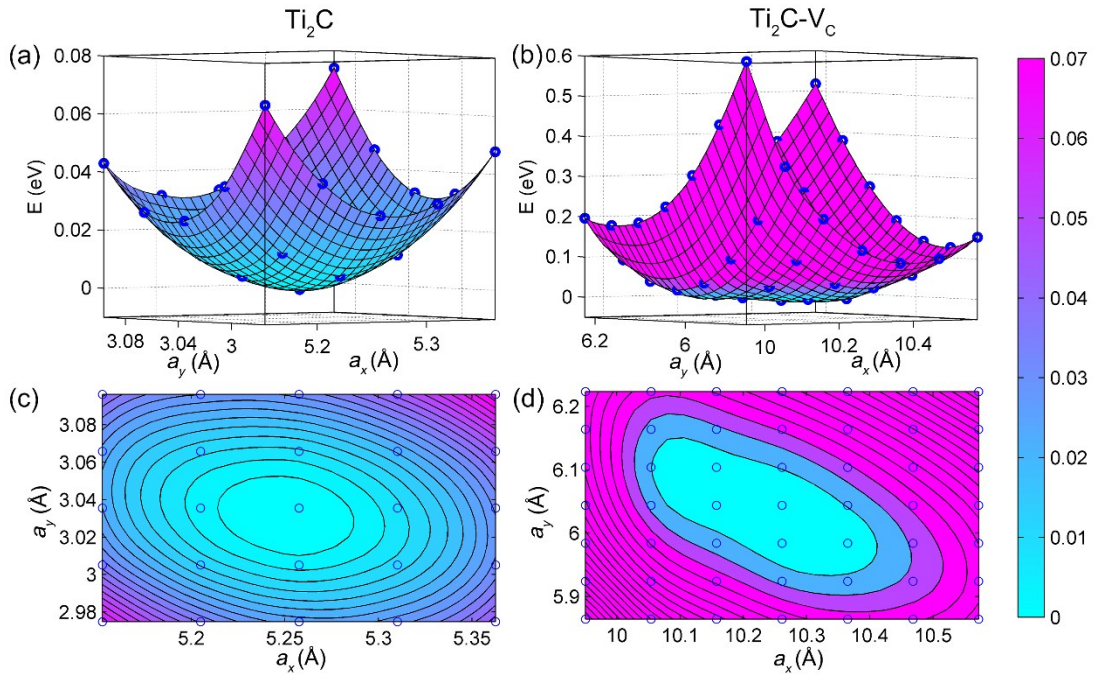


**Fig. S10a**  $V_C$  induced flexibility in  $\text{Ti}_2\text{C}$  MXenes. The three-dimensional plot of  $a_x$ ,  $a_y$  and corresponding strain energies of (a)  $\text{Ti}_2\text{C}$  and (b)  $\text{Ti}_2\text{C}-V_C$ . Contour of energy in the  $a_x$ - $a_y$  plane

of (c)  $\text{Ti}_2\text{C}$  and (d)  $\text{Ti}_2\text{C}-\text{V}_\text{C}$ . The blue balls are actual points and the lines are the fitted formula. Note that the stiffness decreases dramatically by introducing carbon vacancies in  $\text{Ti}_2\text{C}$  MXenes.

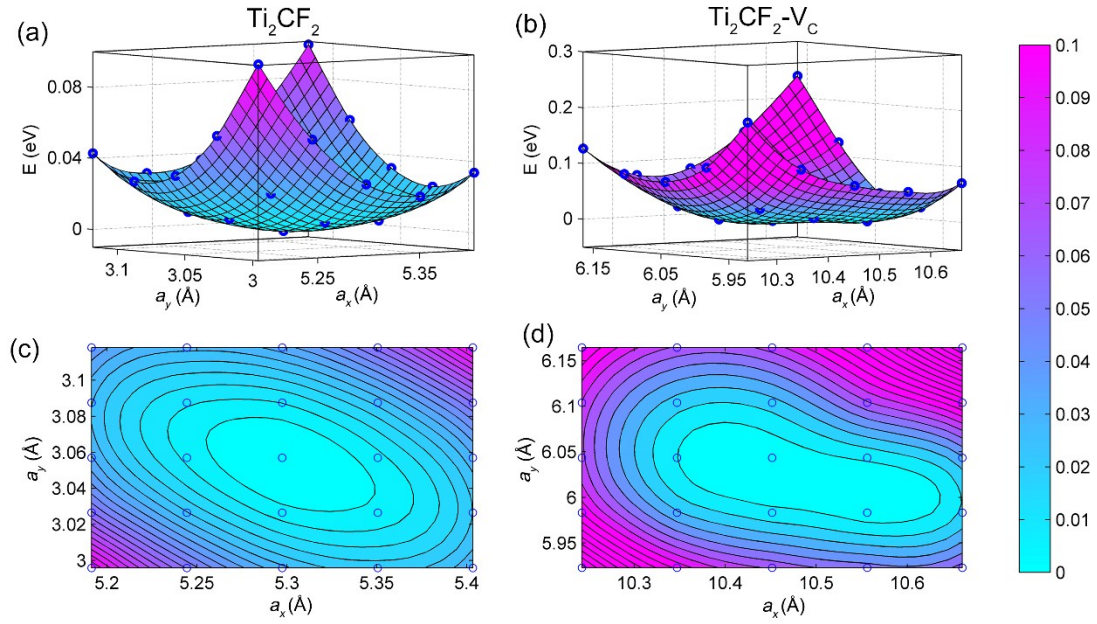


**Fig. S10b**  $\text{V}_\text{C}$  induced flexibility in  $\text{Ti}_2\text{CF}_2$  MXenes. The three-dimensional plot of  $a_x$ ,  $a_y$  and corresponding strain energies of (a)  $\text{Ti}_2\text{CF}_2$  and (b)  $\text{Ti}_2\text{CF}_2-\text{V}_\text{C}$ . Contour of energy in the  $a_x$ - $a_y$  plane of (c)  $\text{Ti}_2\text{CF}_2$  and (d)  $\text{Ti}_2\text{CF}_2-\text{V}_\text{C}$ . The blue balls are actual points and the lines are the fitted formula. Note that the stiffness decreases dramatically by introducing carbon vacancies in  $\text{Ti}_2\text{CF}_2$  MXenes.

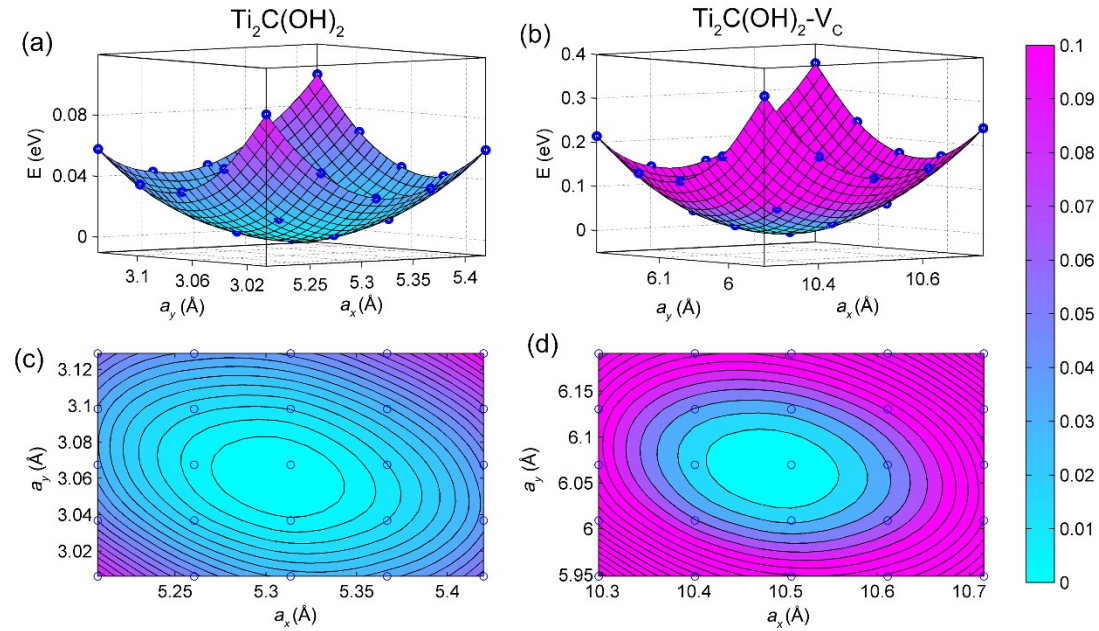


**Fig. S10c**  $\text{V}_\text{C}$  induced flexibility in  $\text{Ti}_2\text{C}(\text{OH})_2$  MXenes. The three-dimensional plot of  $a_x$ ,  $a_y$  and corresponding strain energies of (a)  $\text{Ti}_2\text{C}(\text{OH})_2$  and (b)  $\text{Ti}_2\text{C}(\text{OH})_2-\text{V}_\text{C}$ . Contour of energy in the  $a_x$ - $a_y$  plane of (c)  $\text{Ti}_2\text{C}(\text{OH})_2$  and (d)  $\text{Ti}_2\text{C}(\text{OH})_2-\text{V}_\text{C}$ . The blue balls are actual points and the lines

are the fitted formula. Note that the stiffness decreases dramatically by introducing carbon vacancies in  $\text{Ti}_2\text{C}(\text{OH})_2$  MXenes.

**Table S1.** Formation energy of carbon vacancy ( $E_f(V_C)$ , eV) in  $\text{Ti}_{n+1}\text{C}_n\text{T}_2$  ( $n = 1$  and  $2$ ,  $T = \text{O}, \text{F}$  and  $\text{OH}$ ) monolayer and graphene with the same scheme.

formula	$E_f(V_C)$	formula	$E_f(V_C)$
$\text{Ti}_2\text{C}$	2.51	$\text{Ti}_3\text{C}_2$	2.45
$\text{Ti}_2\text{CO}_2$	0.62	$\text{Ti}_3\text{C}_2\text{O}_2$	0.65
$\text{Ti}_2\text{CF}_2$	2.70	$\text{Ti}_3\text{C}_2\text{F}_2$	1.88
$\text{Ti}_2\text{C}(\text{OH})$	2.25	$\text{Ti}_3\text{C}_2(\text{OH})_2$	1.65

Formation energy of graphene is within the same scheme. A  $2 \times 2 \times 1$  supercell was used.  $E_{\text{tot}}(\text{Graphene}) = -310.1871$  eV, 2 C in a unit cell.  $E_{\text{tot}}(\text{Graphene}-V_C) = -1078.4251$  eV, 7 C in a unit cell, corresponds to a  $V_C$  concentration: 12.5%.  $E(V_C) = E_{\text{tot}}(\text{Graphene}-V_C) - 7 \times (E_{\text{tot}}(\text{Graphene})/2) = 7.23$  eV, agreeing well with earlier work, 7.4 eV.

**Table S2a.** Calculated frequencies of vibrational modes at gamma point in transition states of carbon vacancy migration in  $\text{Ti}_2\text{C}-V_C$ . There are 11 atoms per a unit cell of  $\text{Ti}_2\text{C}-V_C$ , so there are 33 phonon branches, correspondingly, there are 33 vibrational modes at gamma point. Frequency is given in  $\text{cm}^{-1}$ .

mode	frequency	mode	frequency	mode	frequency
1	-290	12	193	23	294
2	0	13	196	24	302
3	0	14	206	25	328
4	0	15	232	26	489
5	112	16	237	27	575
6	130	17	245	28	604
7	138	18	251	29	615
8	147	19	253	30	631
9	161	20	265	31	671
10	167	21	271	32	682
11	185	22	286	33	686

**Table S2b.** Calculated frequencies of vibrational modes at gamma point in transition states of carbon vacancy migration in  $\text{Ti}_2\text{CO}_2\text{-V}_\text{C}$ . There are 19 atoms per a unit cell of  $\text{Ti}_2\text{CO}_2\text{-V}_\text{C}$ , so there are 57 phonon branches, correspondingly, there are 57 vibrational modes at gamma point. Frequency is given in  $\text{cm}^{-1}$ .

mode	frequency	mode	frequency	mode	frequency
1	-250	20	244	39	466
2	0	21	252	40	505
3	0	22	253	41	524
4	0	23	254	42	528
5	55	24	275	43	537
6	94	25	286	44	540
7	116	26	288	45	545
8	131	27	292	46	549
9	149	28	311	47	578
10	155	29	320	48	589
11	168	30	330	49	593
12	175	31	337	50	604
13	192	32	351	51	607
14	199	33	356	52	611
15	205	34	372	53	635
16	217	35	385	54	637
17	221	36	402	55	668
18	230	37	431	56	680
19	240	38	443	57	775

**Table S2c.** Calculated frequencies of vibrational modes at gamma point in transition states of carbon vacancy migration in  $\text{Ti}_2\text{CF}_2\text{-V}_\text{C}$ . There are 19 atoms per a unit cell of  $\text{Ti}_2\text{CF}_2\text{-V}_\text{C}$ , so there are 57 phonon branches, correspondingly, there are 57 vibrational modes at gamma point. Frequency is given in  $\text{cm}^{-1}$ .

mode	frequency	mode	frequency	mode	frequency
1	-392	20	223	39	314
2	0	21	225	40	324
3	0	22	229	41	340
4	0	23	230	42	368
5	62	24	233	43	384
6	131	25	237	44	397
7	137	26	242	45	401
8	153	27	251	46	404
9	156	28	255	47	417
10	162	29	259	48	443
11	181	30	260	49	502
12	184	31	264	50	530
13	189	32	271	51	620
14	194	33	289	52	630
15	200	34	295	53	650
16	201	35	298	54	652
17	205	36	301	55	661
18	216	37	304	56	692
19	217	38	309	57	788

**Table S2d.** Calculated frequencies of vibrational modes at gamma point in transition states of carbon vacancy migration in  $\text{Ti}_2\text{C}(\text{OH})_2\text{-V}_\text{C}$ . There are 27 atoms per a unit cell of  $\text{Ti}_2\text{C}(\text{OH})_2\text{-V}_\text{C}$ , so there are 81 phonon branches, correspondingly, there are 81 vibrational modes at gamma point.

Frequency is given in  $\text{cm}^{-1}$ .

mode	frequency	mode	frequency	mode	frequency
1	-264	28	269	55	529
2	0	29	280	56	538
3	0	30	282	57	544
4	0	31	298	58	562
5	89	32	303	59	572
6	142	33	314	60	579
7	174	34	317	61	583
8	180	35	332	62	596
9	195	36	339	63	613
10	199	37	362	64	621
11	201	38	379	65	639
12	207	39	388	66	640
13	211	40	389	67	641
14	214	41	391	68	652
15	223	42	402	69	657
16	226	43	414	70	661
17	229	44	431	71	699
18	231	45	435	72	705
19	233	46	446	73	847
20	242	47	471	74	3444
21	244	48	478	75	3465
22	250	49	485	76	3560
23	256	50	489	77	3563
24	258	51	495	78	3573
25	259	52	504	79	3576
26	262	53	517	80	3628
27	265	54	523	81	3629

**Table S3.** Stiffness of graphene, MoS<sub>2</sub>, Ti<sub>2</sub>CT<sub>2</sub> and Ti<sub>2</sub>CT<sub>2</sub>-V<sub>C</sub>.

formula	$c_1$	$c_2$	$c_3$	$C$ (N/m)	Poisson's ratio
graphene	114.5	114.9	40.95	337.87	0.18
MoS <sub>2</sub>	71.35	72.31	35.57	122.4	0.25
Ti <sub>2</sub> C	70.9	74.2	30.5	135.53	0.21
Ti <sub>2</sub> C-V <sub>C</sub>	246.2	176.3	216.8	102.52	0.44
Ti <sub>2</sub> CO <sub>2</sub>	133.7	46.12	85.15	241.86	0.17
Ti <sub>2</sub> CO <sub>2</sub> -V <sub>C</sub>	448.7	448.4	280.6	202.24	0.50
Ti <sub>2</sub> CF <sub>2</sub>	86.48	46.12	77.58	136.67	0.45
Ti <sub>2</sub> CF <sub>2</sub> -V <sub>C</sub>	86.24	77.44	85.78	75.91	0.50
Ti <sub>2</sub> C(OH) <sub>2</sub>	97.17	94.45	46.12	179.12	0.24
Ti <sub>2</sub> C(OH) <sub>2</sub> -V <sub>C</sub>	99.28	96.53	49.06	177.23	0.25

#### AIMD details

Structural stability at  $T = 0$ , evidenced in the vibration spectra, says little about stability at high temperatures, where thermally activated structural changes may take place. A more direct way to probe the stability of Ti<sub>2</sub>CT<sub>2</sub>-V<sub>C</sub> at high temperatures is by performing ab initio molecular dynamics (AIMD) simulations. Results of our canonical AIMD simulations are presented as structural snap shots of infinite Ti<sub>2</sub>CT<sub>2</sub>-V<sub>C</sub> monolayers at  $T = 300$  K and  $T = 1000$  K in Fig. S2. To avoid artifacts associated with constraints imposed by finite-size unit cells, we used very large supercells containing 96 atoms for Ti<sub>2</sub>CT<sub>2</sub>-V<sub>C</sub>. Due to the large unit cell size, we needed to limit the simulation time to 1 ps for Ti<sub>2</sub>CT<sub>2</sub>-V<sub>C</sub> when using 1 fs time steps. This simulation time still covers about 10 vibration periods of the optical modes and thus should indicate the propensity to structural changes. At room temperature, we find the structural changes in the layers to be minimal. More significant changes are expected at  $T = 1000$  K. Even though the changes are

larger in this case, they resemble more the onset of a melting process than a concerted structural change. The simulation processes are presented in movies S1–S4.

**Movies S1.** Top view of  $\text{Ti}_2\text{C}-\text{V}_\text{C}$  monolayer endure 1 ps AIMD simulation at 300 K. No structure collapse or reconstruction was found.

**Movies S2.** Side view of  $\text{Ti}_2\text{C}-\text{V}_\text{C}$  monolayer endure 1 ps AIMD simulation at 300 K. No structure collapse or reconstruction was found.

**Movies S3.** Top view of  $\text{Ti}_2\text{C}-\text{V}_\text{C}$  monolayer endure 1 ps AIMD simulation at 1000 K. Obvious structure collapse was observed at around 150 fs.

**Movies S4.** Side view of  $\text{Ti}_2\text{C}-\text{V}_\text{C}$  monolayer endure 1 ps AIMD simulation at 1000 K. Obvious structure collapse was observed at around 150 fs.

**Movies S5.** Top view of  $\text{Ti}_2\text{CO}_2-\text{V}_\text{C}$  monolayer endure 1 ps AIMD simulation at 300 K. No structure collapse or reconstruction was found.

**Movies S6.** Side view of  $\text{Ti}_2\text{CO}_2-\text{V}_\text{C}$  monolayer endure 1 ps AIMD simulation at 300 K. No structure collapse or reconstruction was found.

**Movies S7.** Top view of  $\text{Ti}_2\text{CO}_2-\text{V}_\text{C}$  monolayer endure 1 ps AIMD simulation at 1000 K. No structure collapse or reconstruction was found.

**Movies S8.** Side view of  $\text{Ti}_2\text{CO}_2-\text{V}_\text{C}$  monolayer endure 1 ps AIMD simulation at 1000 K. No structure collapse or reconstruction was found.